heterodimer–ligand complexes were dialysed against a buffer without ligands before ESI-MS analyses.

Received 25 July; accepted 31 October 2001.

1. Bourguet, W., Germain, P. & Gronemeyer, H. Nuclear receptor ligand-binding domains: three-dimensional structures, molecular interactions and pharmacological implications. *Trends Pharmacol. Sci.* **21,** 381–388 (2000).
2. Glass, C. K. & Rosenfeld, M. G. The coregulator exchange in transcriptional functions of nuclear receptors. *Genes Dev.* **14,** 121–141 (2000).
3. Freedman, L. P. Increasing the complexity of coactivation in nuclear receptor signaling. *Cell* **97,** 5–8 (1999).
4. Kurokawa, R. *et al.* Regulation of retinoid signalling by receptor polarity and allosteric control of ligand binding. *Nature* **371,** 528–531 (1994).
5. Forman, B. M., Umesono, K., Chen, J. & Evans, R. M. Unique response pathways are established by allosteric interactions among nuclear hormone receptors. *Cell* **81,** 541–550 (1995).
6. Chen, J. Y. *et al.* Two distinct actions of retinoid-receptor ligands. *Nature* **382,** 819–822 (1996).
7. Vivat, V. *et al.* A mutation mimicking ligand-induced conformational change yields a constitutive RXR that senses allosteric effects in heterodimers. *EMBO J.* **16,** 5697–5709 (1997).
8. Roy, B., Taneja, R. & Chambon, P. Synergistic activation of retinoic acid (RA)-responsive genes and induction of embryonal carcinoma cell differentiation by an RA receptor alpha (RARα)-, RARβ-, or RARγ-selective ligand in combination with a retinoid X receptor-specific ligand. *Mol. Cell. Biol.* **15,** 6481–6487 (1995).
9. Voegel, J. J. *et al.* The coactivator TIF2 contains three nuclear receptor-binding motifs and mediates transactivation through CBP binding-dependent and -independent pathways. *EMBO J.* **17,** 507–519 (1998).
10. Lehmann, J. M. *et al.* Retinoids selective for retinoid X receptor response pathways. *Science* **258,** 1944–1946 (1992).
11. Voegel, J. J., Heine, M. J. S., Zechel, C., Chambon, P. & Gronemeyer, H. TIF2, a 160 kDa transcriptional mediator for the ligand-dependent activation function AF-2 of nuclear receptors. *EMBO J.* **15,** 3667–3675 (1996).
12. Westin, S. *et al.* Interactions controlling the assembly of nuclear-receptor heterodimers and co-activators. *Nature* **395,** 199–202 (1998).
13. Klein, E. S. *et al.* Identification and functional separation of retinoic acid receptor neutral antagonists and inverse agonists. *J. Biol. Chem.* **271,** 22692–22696 (1996).
14. Chen, J. D. & Evans, R. M. A transcriptional co-repressor that interacts with nuclear hormone receptors. *Nature* **377,** 454–457 (1995).
15. Hu, X. & Lazar, M. A. The CoRNR motif controls the recruitment of corepressors by nuclear hormone receptors. *Nature* **402,** 93–96 (1999).
16. Nagy, L. *et al.* Mechanism of corepressor binding and release from nuclear hormone receptors. *Genes Dev.* **13,** 3209–3216 (1999).
17. Perissi, V. *et al.* Molecular determinants of nuclear receptor-corepressor interaction. *Genes Dev.* **13,** 3198–3208 (1999).
18. Hu, X., Li, Y. & Lazar, M. A. Determinants of CoRNR-dependent repression complex assembly on nuclear hormone receptors. *Mol. Cell. Biol.* **21,** 1747–1758 (2001).
19. Cohen, R. N. *et al.* The specificity of interactions between nuclear hormone receptors and corepressors is mediated by distinct amino acid sequences within the interacting domains. *Mol. Endocrinol.* **15,** 1049–1061 (2001).
20. Wong, C. W. & Privalsky, M. L. Transcriptional silencing is defined by isoform- and heterodimer-specific interactions between nuclear hormone receptors and corepressors. *Mol. Cell. Biol.* **18,** 5724–5733 (1998).
21. Bourguet, W. *et al.* Crystal structure of a heterodimeric complex of RAR and RXR ligand-binding domains. *Mol. Cell* **5,** 289–298 (2000).
22. Yang, W., Rachez, C. & Freedman, L. P. Discrete roles for peroxisome proliferator-activated receptor gamma and retinoid X receptor in recruiting nuclear receptor coactivators. *Mol. Cell. Biol.* **20,** 8008–8017 (2000).
23. Hittelman, A. B., Burakov, D., Iniguez-Lluhi, J. A., Freedman, L. P. & Garabedian, M. J. Differential regulation of glucocorticoid receptor transcriptional activation via AF-1-associated proteins. *EMBO J.* **18,** 5380–5388 (1999).
24. Benecke, A., Chambon, P. & Gronemeyer, H. Synergy between estrogen receptor a activation functions AF1 and AF2 mediated by transcription intermediary factor TIF2. *EMBO Rep.* **1,** 151–157 (2000).
25. Alen, P., Claessens, F., Verhoeven, G., Rombauts, W. & Peeters, B. The androgen receptor amino-terminal domain plays a key role in p160 coactivator-stimulated gene transcription. *Mol. Cell. Biol.* **19,** 6085–6097 (1999).
26. Yang, W. & Freedman, L. P. 20-Epi analogues of 1,25-dihydroxyvitamin D3 are highly potent inducers of DRIP coactivator complex binding to the vitamin D3 receptor. *J. Biol. Chem.* **274,** 16838–16845 (1999).
27. Nagpal, S., Friant, S., Nakshatri, H. & Chambon, P. RARs and RXRs: evidence for two autonomous transactivation functions (AF-1 and AF-2) and heterodimerization *in vivo*. *EMBO J.* **12,** 2349–2360 (1993).
28. Iyer, J. *et al.* Versatile copurification procedure for rapid isolation of homogeneous RAR-RXR heterodimers. *Protein Expr. Purif.* **16,** 308–314 (1999).
29. Bourguet, W. *et al.* Heterodimeric complex of RAR and RXR nuclear receptor ligand-binding domains: purification, crystallization, and preliminary X-ray diffraction analysis. *Protein Expr. Purif.* **19,** 284–288 (2000).
30. Chen, J. *et al.* RAR-specific agonist antagonists which dissociate transactivation and AP1 transrepression inhibit anchorage-independent cell proliferation. *EMBO J.* **14,** 1187–1197 (1995).

Acknowledgements

We thank W. Raffelsberger for providing the PCR protocols for RARβ2 promoter amplification, and N. Potier and A. van Dorsselaer for the ESI-MS analysis. We are grateful to C. Peluso-Iltis and V. Chavant for help in protein purification, C. Erb for expression vectors and A. Pornon for technical assistance. We thank W. Bourguet for critically reading this manuscript and Y. Lutz and C. Egly for antibodies. BMS-labelled retinoids/rexinoids were provided by C. Zusi, and CD3254 and AGN192870 by U. Reichert and S. Michel. This work was supported by the Institut National de la Santé et de la Recherche Médicale, the Centre National de La Recherche Scientifique, the Hôpital Universitaire de Strasbourg, the European Community and Bristol-Myers Squibb.

Competing interests statement

The authors declare that they have no competing financial interests.

Correspondence and requests for materials should be addressed to H.G. (e-mail: hg@igbmc.u-strasbg.fr).

The motor domain determines the large step of myosin-V

Hiroto Tanaka*, Kazuaki Homma†, Atsuko Hikikoshi Iwane‡, Eisaku Katayama§‖, Reiko Ikebe†, Junya Saito†, Toshio Yanagida*‡ & Mitsuo Ikebe†

* *Single Molecule Processes Project, ICORP, JST, 2-4-14, Senba-higashi, Mino, Osaka 562–0035, Japan*
† *Department of Physiology, University of Massachusetts Medical School, 55 Lake Avenue North, Worcester, Massachusetts 01655-0127, USA*
‡ *Department of Physiology and Biosignaling, Graduate School of Medicine Osaka University, 2-2, Yamadaoka, Suita, Osaka, 565–0871, Japan*
§ *Division of Biomolecular Imaging, Institute of Medical Science, The University of Tokyo, Minato-ku, Tokyo, 108-8639, Japan*
‖ *PRESTO, Japan Science and Technology Corporation, Kawaguchi, Saitama 332-0012, Japan*

Class-V myosin proceeds along actin filaments with large (~36 nm) steps[1–3]. Myosin-V has two heads, each of which consists of a motor domain and a long (23 nm) neck domain. In accordance with the widely accepted lever-arm model[4], it was suggested that myosin-V steps to successive (36 nm) target zones along the actin helical repeat by tilting its long neck (lever-arm)[5]. To test this hypothesis, we measured the mechanical properties of single molecules of myosin-V truncation mutants with neck domains only one-sixth of the native length. Our results show that the processivity and step distance along actin are both similar to those of full-length myosin-V. Thus, the long neck domain is not essential for either the large steps or processivity of myosin-V. These results challenge the lever-arm model. We propose that the motor domain and/or the actomyosin interface enable myosin-V to produce large processive steps during translocation along actin.

Structural studies of myosin in crystal[6] and solution[7,8] have shown that the angle of the neck domain of the myosin head relative to the motor domain changes, depending on the form of bound nucleotide, as a result of the conformational change in the motor domain. On the basis of these findings, a lever-arm model has been proposed, in which the neck domain acts as a lever-arm and the movement is caused by the tilting neck domain[4]. This model postulates that the displacement and the velocity of myosin are proportional to the length of the neck domain. To test this model, the displacement and sliding velocity of intact and biochemically modified myosin, which have different lengths of neck domains, has been measured. However, not all of the results are consistent with this model; some investigators have shown that the displacement[9,10] and velocity[9,11] are proportional to the neck domain length, but others have shown that the neck domain length does not affect the velocity[12–15]. Myosin-V, which has a long neck domain (two to three times as large as those of conventional myosin-II), moves on an actin filament for a long distance with many successive large steps (~36 nm) without dissociating from actin, called processive

movement[1,3]. The large steps and processivity of myosin-V make it possible to determine the displacement and movement of individual myosin-V molecules more directly and precisely. We thus studied the mechanism of myosin movement using myosin-V and its truncation mutants.

We constructed a chimaera of the head region of myosin-V attached to the chicken smooth-muscle myosin rod, in which five out of six calmodulin-binding 'IQ-domains' (IQ-motifs) in the neck region were truncated (M5IQ1rod; Fig. 1a). The actin translocating velocity, which is driven by multiple M5IQ1rods bound to a glass surface (surface assay), was 0.30 ± 0.10 μm s^{-1} (± standard deviation; $n = 132$). This was similar to previously reported actin velocities driven by wild-type myosin-V (ref. 1) and recombinant myosin-V fragments—HMM and S1—fully-equipped with six IQ-motifs[13,15,16]. For control experiments, a M5IQ6rod containing six intact IQ-motifs, a long neck of myosin-V, and a smooth-muscle myosin rod was also constructed (Fig. 1b). M5IQrods and M5IQ6rods were co-polymerized into 5–8-μm filaments with rabbit skeletal-muscle myosin rods. During the co-polymerization, we incubated the skeletal-muscle myosin rods at larger molar excess than for the M5IQ1rods or M5IQ6rods to ensure that only a few M5IQ1rods or M5IQ6rods were included in each cofilament. Cofilaments were sparsely adsorbed onto the surface of a pedestal made on a glass surface[17,18] (Fig. 2a). The number of M5IQ1rods or M5IQ6rods in a cofilament was checked by observing single fluorescent nucleotide analogues (Cy3-ATP or Cy3-ADP) bound to M5IQ1rods or M5IQ6rods[17,18] (Fig. 2b). The use of long cofilaments not only allowed us easily to find the location of M5IQ1rods or M5IQ6rods on the glass surface, but also avoided any damage to them caused by interaction with the glass. An actin filament with both ends attached to optically trapped beads was brought into contact with single M5IQ1rods or M5IQ6rods in a cofilament, and individual displacement events were determined by measuring bead displacements with nanometre accuracy (Fig. 2a) as previously described[17–20].

We observed the mechanical events of single M5IQ1rods and M5IQ6rods at 2 mM ATP. Figure 3a and b show typical recordings of the displacements of M5IQ1rods and M5IQ6rods, respectively. Displacements occurred in steps (Fig. 3a, b, arrows). Most of the displacements of both myosins took place in one direction (defined as forward). In the 'falling' phase, many (~60%) of the displacements abruptly returned to zero displacement without steps (Fig. 3a left, b), indicating that the myosin dissociated from the actin filament, while others returned to zero in a stepwise fashion (Fig. 3a, right). The start position of the displacement cannot be determined because it is randomized owing to the thermal motion of the beads[20]. Therefore, the size of the first step was determined by averaging many steps, in which the start position was averaged to be zero displacement[20] (insets to Fig. 3a left and b). The averaged size of the first step was 25 nm for a M5IQ1rod and 20 nm for a M5IQ6rod. The start positions of the second and third steps could be determined (Fig. 3a, b), so the size of individual steps was measured directly. Figure 3c shows a histogram of the step size of a M5IQ1rod in the forward and backward directions (the first steps were not included). The mean sizes of the forward and backward steps were both approximately 35 nm. Most of the backward steps took place in

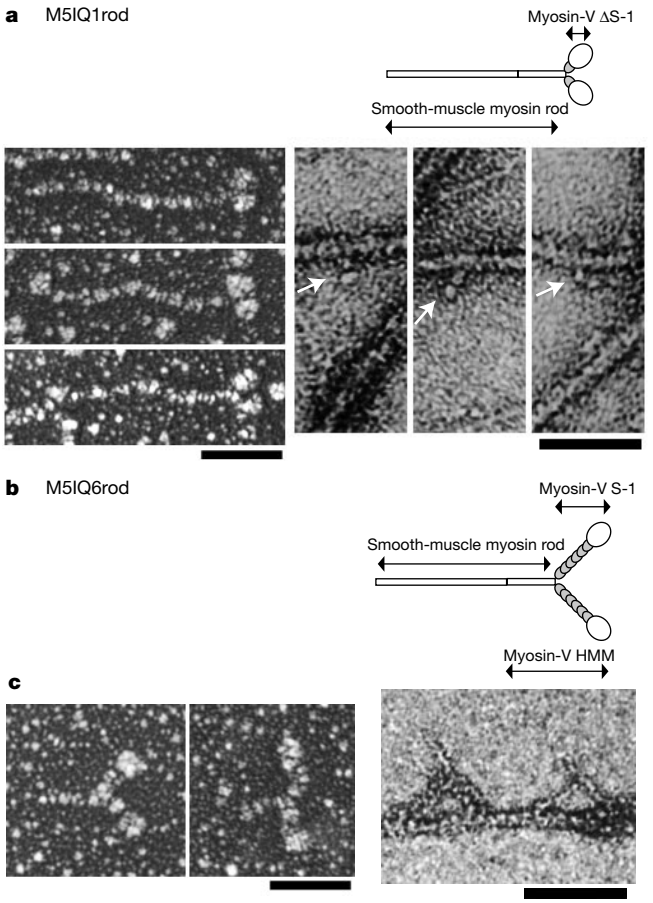

Figure 1 Structure of the deletion mutant of myosin-V (M5IQ1rod). **a**, Diagram of the M5IQ1rod (top). The M5IQ1rod consists of the two deletion heads of myosin-V (a motor domain plus one IQ-motif for each head (ΔS-1)) and the long coiled-coil tail (rod) of chicken smooth-muscle myosin. Rotary-shadowed electron microscopic images of M5IQ1rods (lower left). Negatively stained images of M5IQ1rods interacting with actin filaments (lower right). Myosins interacted with actin filaments in assay buffer containing approximately 5 μM ATP, then the assay buffer was rapidly replaced by staining solution[28]. The arrows indicate M51Qrod molecules interacting with actin filaments. Scale bars indicate 50 nm. **b**, Diagram of the M5IQ6rod (M5IQ6 contains six intact IQ-motifs). **c**, Rotary-shadowed electron microscopic images of myosin-V HMM (see **b**) (left) and negatively stained images of its complexes with actin filaments (right). The negatively stained images, taken under the same conditions as those in **a**, were consistent with those of myosin-V HMM previously reported[5].

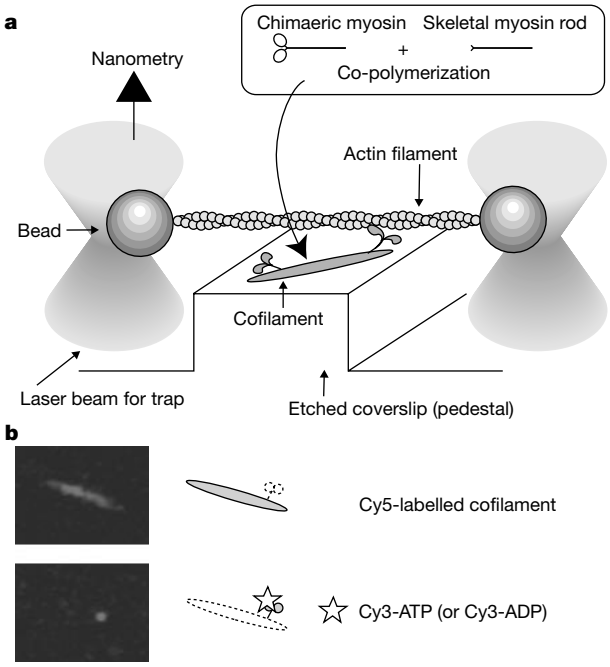

Figure 2 Single-molecule measurement of displacements. **a**, Diagram of the measurement system for displacements. **b**, Fluorescence images (with corresponding diagrams) of a cofilament (top) and Cy3 nucleotides bound to M5IQ1rod in the cofilament (bottom); see text. A single M5IQ1rod molecule was incorporated into a cofilament.

the falling phase, that is, passively (Fig. 3c, grey bars), but a small number of backward steps developed against the force owing to the optically trapped bead (Fig. 3c, black bars). The ratio of forward steps to backward steps that developed against the force (Fig. 3c, black bars) was 10:1. We observed 56 displacements in which two successive 35-nm steps took place against the trap force in the forward direction, but we never observed such a displacement in the backward direction.

Figure 3d shows a histogram of dwell times between the adjacent forward steps of a M5IQ1rod. The mean dwell time for forward steps was 0.11 s. The velocity of forward displacements calculated as (mean step size)/(mean dwell time) was equal to 320 nm s^{-1} (= 35 nm/0.11 s). This value was consistent with that in the surface-gliding assay for a M5IQ1rod. The dwell times for the last steps were not included because the optical trap force stalled the movement of the M5IQ1rod (Fig. 3a, b).

The step size, processivity, and the dwell time of a M5IQ6rod were all similar to those of a M5IQ1rod (Fig. 3b). The step sizes (35 nm) of M5IQ1rods and M5IQ6rods were consistent with that of wild-type myosin-V (refs 1, 3). The result clearly indicates that the large lever-arm length of myosin-V is not a determinant of its large step size. The M5IQ6rod underwent backward steps similarly to the M5IQ1rod. Backward steps have been reported for wild-type myosin-V (refs 1, 3) as well.

A maximum number of three processive steps was observed; back steps were sometimes observed. Therefore, it could be argued that the large noise in Fig. 3a and b is caused by the thermal forwards and backwards bouncing motion of the actin filament when it is released from myosin, so the myosin just binds to appropriate monomers presented in the correct orientation every 36 nm. This might be the case, if the load is nearly zero, but the trapping force exerted on the myosin was large in our assay. Because the trap stiffness was 0.02 pN nm^{-1}, if the starting position is zero displacement, the force increases from 0 to 0.4 pN at the first step, from 0.4 to 1.1 pN at the second step and from 1.1 to 1.8 pN at the third step. The energy required for generating the fourth step, if possible, is given as 35 nm × (1.8 + 2.5) pN/2 = 75 pN nm^{-1}, which is similar to the energy of ATP hydrolysis[21]. If the efficiency is similar to that of muscle myosin (~50%), it is reasonable not to expect more than three processive steps.

Furthermore, the probability that two successive 35-nm steps are thermally produced against the force of over 1 pN in one direction is extremely small: less than $\exp(-35\ \text{nm per step} \times 2\ \text{steps} \times 1\ \text{pN}/k_B T) = 10^{-8}$. We observed two such successive 35-nm steps 56 times, but only in the forward direction. Thus, the observed steps must be actively caused using the energy from ATP hydrolysis. The noise in Fig. 3a and b can be explained by the large compliance (1/stiffness) of the bead–actin filament junction[22]. That is why the noise did not decrease much when the myosin attached to an actin filament.

Many (more than 3) processive steps of wild-type myosin-V have been observed[3]. This would not be because the wild-type myosin-V was used, but because the load was low (the load was controlled to be relatively small (1 pN) using feedback-enhanced optical trapping nanometry). A wild-type myosin-V also produced a number of steps similar to the present study when the steps were measured by optical trapping nanometry without feedback[1].

When the concentration of ATP was decreased to [ATP] = 1 μM, the displacements of M5IQ1rods also developed in a stepwise fashion as well (data not shown). The size of step (mean, 35 nm) was similar to that at 2 mM. The dwell time, however, increased to 1.7 s. At 1 μM ATP, the binding of ATP to an acto-M5IQ1rod complex would be a rate-limiting step. The second-order binding constant of ATP calculated as 1/[ATP](dwell time) = 0.6 $\mu M^{-1}\ s^{-1}$. This value is consistent with the kinetic analyses for myosin-V with six IQ motifs[3,13,15,16,23].

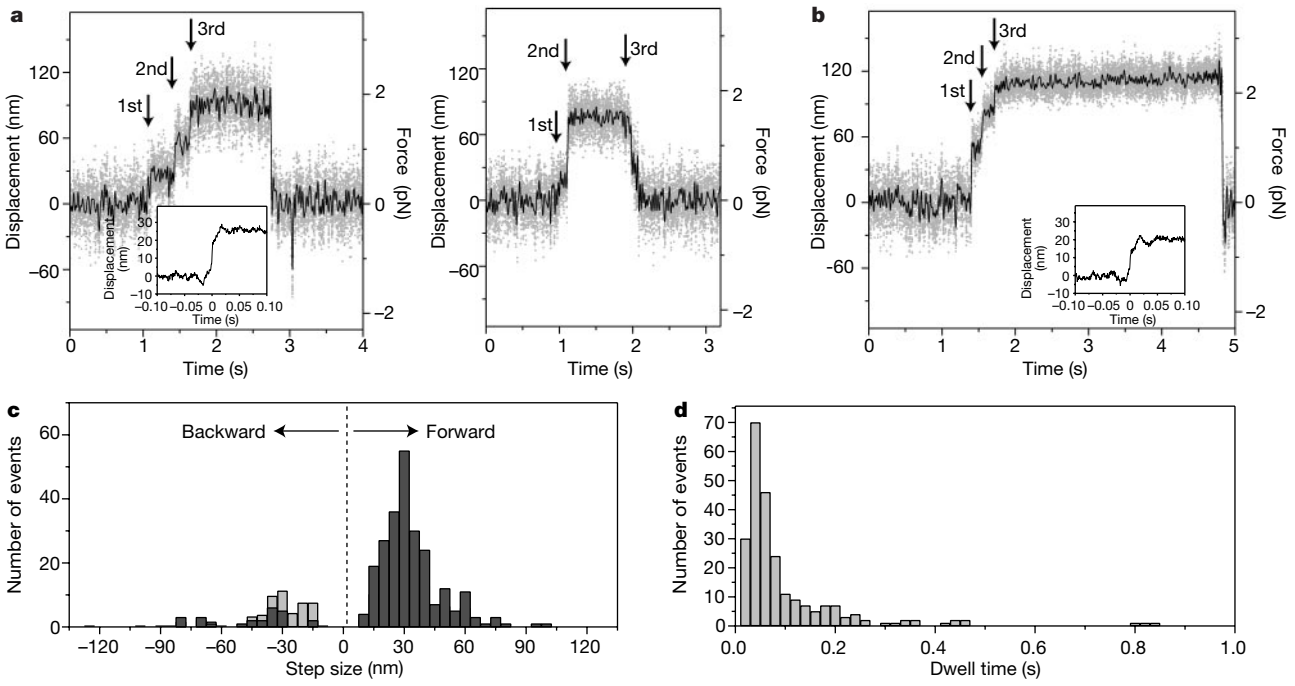

Figure 3 Records of displacements at a high ATP concentration of 2 mM. Typical records of the time courses of generation of displacements by single M5IQ1rods (**a**, right and left) and M5IQ6rods (**b**). Grey dots, raw data. Black line, data passed through a low-pass filter of 30-Hz bandwidth. Arrows indicate positions of steps. Insets in **a** and **b** are averaged traces of first steps (see text). **c**, Histogram of step size of a M5IQ1rod. In the backward direction, black and grey bars indicate the numbers of steps that developed against the force owing to the optically trapped bead and in the falling phase (passive steps), respectively (see text for detail). The large step sizes of >60 nm are probably due to two successive steps that took place rapidly within the temporal resolution (1.6 ms) of the measurement system (see the second step in **a**, right). **d**, Histogram of dwell times of steps of M5IQ1rod in the forward direction. Medium: 25 mM KCl, 5 mM $MgCl_2$, 1 mM EGTA, 0.2 mg ml^{-1} calmodulin, 2 mM ATP and 20 mM HEPES (pH 7.8). The medium contained 4 μM phalloidin to stabilize actin filaments and an oxygen scavenger system to reduce photobleaching[17]. Trap stiffness, 0.02 pN nm^{-1}. Temperature, 30 °C.

Thus the size, processivity, and velocity of steps of the M5IQ1rods were essentially the same as those obtained for M5IQ6rods and previously reported for intact myosin-V (ref. 1) fully equipped with six IQ motifs. The step size of myosin-V coincides with the actin helical pitch (36 nm) and its two heads span the actin helical pitch of actin filaments in electron micrographs[5]. We also observed this in images of myosin-V equipped with an entire IQ domain (see Fig. 1c right). On the basis of these findings, a model was proposed for the processive movement of myosin-V in which myosin-V steps along the helical repeat of an actin filament by tilting the long neck domain of one head and leading the partner head to the neighbouring helical pitch[5]. This model is consistent with the lever-arm model[4]. However, the M5IQ1rod cannot step processively in this way, because its neck domain is too short to span the actin helical pitch. In fact, electron microscopy revealed that most M5IQ1rod molecules appeared to bind to an actin filament with either head and the heads of single molecules do not span the helical pitch (Fig. 1a right).

How can the M5IQ1rod, with its short neck domain, develop such large and processive steps? Perhaps an M5IQ1rod kicks the actin filament to bring the next binding site to it. This is, however, impossible because the inertia of the actin filament and beads is negligibly small. The two heads of the M5IQ1rod are connected at the far ends of their neck domains, away from the actin-binding site, to a coiled-coil rod. Therefore, it is possible that if the coiled coil is untwisted, the two heads could span the helical pitch of an actin filament. However, this is unlikely to occur, because electron microscopy revealed that the two heads of an M5IQ1rod, both in the presence and absence of actin filaments, were rigidly connected at their necks (Fig. 1a, lower left and lower right, respectively). Thus, the M5IQ1 rod does not appear to step along the helical repeats of an actin filament.

The most probable mechanism for the movement of the M5IQ1rod is that the head continuously and rapidly slides along an actin filament to develop an overall large step. The rotation of actin within a step (10 ms) is less than 15 degrees, using the rotational stiffness of an actin filament and the rotational drag of beads[24]. Therefore, the head of an M5IQ1rod fixed on a glass surface could not interact continuously with one protofilament of a double-stranded helix of an actin filament. Consequently, to move continuously between the helical repeats, the M5IQ1rod molecule needs to change the tracks from one protofilament to the other, at the cross-point of the helix. It is plausible that M5IQ1rod, having two heads, slides on the one actin protofilament with one of the two heads, and switches over to the other protofilament with the partner head at the cross-point. The fact that the step size coincides with the helical repeat (36 nm) may be because the sliding of one head of M5IQ1rod on an actin protofilament pauses at the cross-point. The unidirectional movement of myosin heads along the actin helical pitch may be caused through a potential slope made along the helical pitch of an actin filament via its conformational change upon myosin binding. □

Methods

Proteins

Actin and myosin rods were obtained from rabbit skeletal muscle and purified[17]. Recombinant calmodulin from *Xenopus* oocytes was expressed in *Escherichia coli* as described[25].

Generation of the expression vectors for myosin-V constructs

Mouse myosin-V complementary DNA clones were supplied by N. Jenkins[26]. A baculovirus transfer vector for mouse myosin-V variants in pBluebac4 (Invitrogen) was produced as follows. A cDNA fragment (1-3,578) was excised with *Nhe*1/*Kpn*1 digestion and in-frame ligated to a pBluebac4His baculovirus transfer vector containing a hexahistidine tag sequence with a stop codon at the 3′ side of the *Kpn*1 site (M5IQ6 HMM). To obtain single headed myosin-V with one IQ-motif, a *Kpn*1 site was created at nucleotide 2,392. The vector was digested with *Kpn*1 then self-ligated (M5IQ1S1). To produce M5IQ1rod, a *Spe*1 site was created at the 5′ side of the unique *Kpn*1 site of M5IQ1S1 and chicken smooth muscle myosin heavy-chain cDNA fragment (3,325–5,812) flanked with a *Spe*1 and a *Kpn*1 site was inserted to *Spe*1/*Kpn*1 sites at the 3′ side of M5IQ1S1. To produce M5IQ6rod, a *Spe*1 site was created at nucleotide 2,770 of M5IQ6 HMM and the cDNA fragment encoding a smooth-muscle myosin rod flanked with a *Spe*1 and a *Kpn*1 site was inserted into the *Spe*1/*Kpn*1 site of M5IQ6 HMM. For all constructs, a *Spe*1 site was mutated to restore the authentic amino acid residues.

Preparation of recombinant myosin-V

to express recombinant myosin-V, Sf9 cells (about 1×10^9) were co-infected with two separate viruses expressing the myosin-V heavy chain and calmodulin, respectively, as previously described[27]. No contamination of endogenous myosin-V was observed in an SDS–polyacrylamide gel electrophoresis (PAGE) or in rotary-shadowed electron microscope observation of over 200 molecules.

Received 1 August; accepted 18 October 2001.

1. Mehta, A. D. *et al.* Myosin-V is a processive actin-based motor. *Nature* **400,** 590–593 (1999).
2. Sakamoto, T., Amitani, I., Yokota, E. & Ando, T. Direct observation of processive movement by individual myosin V molecules. *Biochem. Biophys. Res. Commun.* **272,** 586–590 (2000).
3. Rief, M. *et al.* Myosin-V stepping kinetics: A molecular model for processivity. *Proc. Natl Acad. Sci. USA* **97,** 9482–9486 (2000).
4. Spudich, J. A. How molecular motors work. *Nature* **372,** 515–518 (1994).
5. Walker, M. L. *et al.* Two-headed binding of a processive myosin to F-actin. *Nature* **405,** 804–807 (2000).
6. Cooke, R. Myosin structure: does the tail wag the dog? *Curr. Biol.* **9,** R773–R775 (1993).
7. Wakabayashi, K. *et al.* Small-angle synchrotron X-ray scattering reveals distinct shape changes of the myosin head during hydrolysis of ATP. *Science* **258,** 443–447 (1992).
8. Corrie, J. E. *et al.* Dynamic measurement of myosin light-chain-domain tilt and twist in muscle contraction. *Nature* **400,** 425–430 (1999).
9. Warshaw, D. M. *et al.* The light chain binding domain of expressed smooth muscle heavy meromyosin acts as a mechanical lever. *J. Biol. Chem.* **275,** 37167–371672 (2000).
10. Ruff, C., Furch, M., Brenner, B., Manstein, D. J. & Meyhofer, E. Single-molecule tracking of myosins with genetically engineered amplifier domains. *Nature Struct. Biol.* **8,** 226–229 (2001).
11. Uyeda, T. Q., Abramson, P. D. & Spudich, J. A. The neck region of the myosin motor domain acts as a lever arm to generate movement. *Proc. Natl Acad. Sci. USA* **93,** 4459–4464 (1996).
12. Itakura, S. *et al.* Force-generating domain of myosin motor. *Biochem. Biophys. Res. Commun.* **196,** 1504–1510 (1993).
13. Trybus, K. M., Krementsova, E. & Freyzon, Y. Kinetic characterization of a monomeric unconventional myosin V construct. *J. Biol. Chem.* **274,** 27448–27456 (1999).
14. Perreault-Micale, C., Shushan, A. D. & Coluccio, L. M. Truncation of a mammalian myosin I results in loss of Ca^{2+}-sensitive motility. *J. Biol. Chem.* **275,** 21618–21623 (1999).
15. Homma, K., Saito, J., Ikebe, R. & Ikebe, M. Ca(2+)-dependent regulation of the motor activity of myosin V. *J. Biol. Chem.* **275,** 34766–347671 (2000).
16. Wang, F. *et al.* Effect of ADP and ionic strength on the kinetic and motile properties of recombinant mouse myosin V. *J. Biol. Chem.* **275,** 4329–4335 (2000).
17. Tanaka, H., Ishijima, A., Honda, M., Saito, K. & Yanagida, T. Orientation dependence of displacements by a single one-headed myosin relative to the actin filament. *Biophys. J.* **75,** 1886–1894 (1998).
18. Ishijima, A. *et al.* Simultaneous observation of individual ATPase and mechanical events by a single myosin molecule during interaction with actin. *Cell* **92,** 161–171 (1998).
19. Finer, J. T., Simmons, R. M. & Spudich, J. A. Single myosin molecule mechanics: piconewton forces and nanometre steps. *Nature* **368,** 113–119 (1994).
20. Molloy, J. E., Burns, J. E., Kendrick-Jones, J., Tregear, R. T. & White, D. C. Movement and force produced by a single myosin head. *Nature* **378,** 209–212 (1995).
21. Stryer, L. *Biochemistry* 4th edn, 443–462 (Freeman, New York, 1995).
22. Dupuis, D. E., Guilford, W. H., Wu, J. & Warshaw, D. M. Actin filament mechanics in the laser trap. *J. Muscle Res. Cell Motil.* **18,** 17–30 (1997).
23. De La Cruz, E. M., Wells, A. L., Rosenfeld, S. S., Ostap, E. M. & Sweeney, H. L. The kinetic mechanism of myosin V. *Proc. Natl Acad. Sci. USA* **96,** 13726–13731 (1999).
24. Tsuda, Y., Yasutake, H., Ishijima, A. & Yanagida, T. Torsional rigidity of single actin filaments and actin-actin bond breaking force under torsion measured directly by in vitro micromanipulation. *Proc. Natl Acad. Sci. USA* **93,** 12937–12942 (1996).
25. Ikebe, M. *et al.* A hinge at the central helix of the regulatory light chain of myosin is critical for phosphorylation-dependent regulation of smooth muscle myosin motor activity. *J. Biol. Chem.* **273,** 17702–17707 (1998).
26. Mercer, J. A., Seperack, P. K., Strobel, M. C., Copeland, N. G. & Jenkins, N. A. Novel myosin heavy chain encoded by murine dilute coat colour locus. *Nature* **349,** 709–713 (1991).
27. Homma, K., Yoshimura, M., Saito, J., Ikebe, R. & Ikebe, M. The core of the motor domain, not the lever-arm/converter domain, determines the direction of myosin movement. *Nature* **412,** 831–834 (2001).
28. Katayama, E. The effects of various nucleotides on the structure of actin-attached myosin subfragment-1 as studied by quick-freeze deep-etch electron microscopy. *J. Biochem.* **106,** 751–770 (1989).

Acknowledgements

We are grateful to N. Jenkins for providing cDNA fragments of mouse myosin-V. We thank colleagues at the Single Molecule Processes Project, University of Massachusetts Medical School, and Osaka University for discussions, and J. West for critically reading the manuscript. This work was supported by grants from the National Institute of Health to M.I.

Correspondence and requests for materials should be addressed to T.Y. (e-mail: yanagida@phys1.med.osaka-u.ac.jp) or M.I. (e-mail: mitsuo.ikebe@umassmed.edu).